13

Synthesis of Palladium-Based Supported Catalysts by Colloidal Oxide Chemistry

Blaise Didillon[a], Thierry Pagès[c], Stephan Verdier[b], and Denis Uzio[c,*]

13.1. INTRODUCTION

In the field of heterogeneous catalysis, the control of the characteristics of supported particles is one of the main objectives of all researchers who want to establish relationships between structure and reactivity. Catalysts with the same macroscopic composition may exhibit very different catalytic performances because of large variations of the active site properties at the nanometer scale. Because of the structure sensitive nature of most of the phenomena involved in heterogeneous catalysis, future improvements of heterogeneous catalysts, in terms of reaction rate, selectivity, stability in operation or sensitivity to poisons, will necessarily be obtained through the nanoscaled control of the physical and chemical characteristics of active sites. For this purpose, many sophisticated preparation methods have been explored including controlled surface reactions such as redox reactions, electrochemical methods, and surface grafting or physical techniques such as vapor deposition of metallic precursors. Chemical methods to prepare supported heterogeneous catalysts generally use the different possible

[a] RHODIA, PPD, P.O. Box 9837 Oldbury, West Midlands, B69 4WD, UK
[b] RHODIA, CRA 52, rue de la Haie Coq 93308 Aubervilliers Cedex, France
[c] IFP Solaize BP no. 3, 69390 Vernaison, France
* To whom correspondence should be addressed. E-mail: denis.uzio@ifp.fr

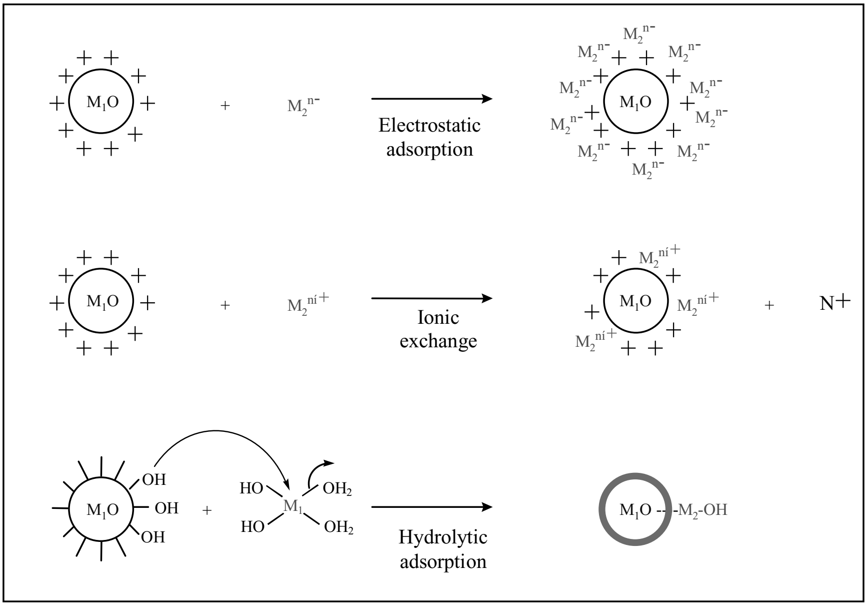

FIGURE 13.1. Different modes of adsorption between metallic precursor and the oxide surface.

interactions between metallic precursors such as ionic complexes (chlorides, amino, sulfates), alkoxides (ethoxy, acetylacetonate), organometallics (allyls, carbonyls) and the surface of an inorganic carrier's hydroxyl groups or Lewis acid sites (uncoordinated sites CUS).[1,2] Ionic exchange, electrostatic interaction, and hydrolytic adsorption may be generated by choosing the right candidates and the appropriate operating conditions, especially pH (Fig. 13.1).

Chemical interactions, often called "grafting," between the surface sites of a carrier and an organometallic or alkoxide compound govern the final particle size distribution for very small particles.[3–5]

However, it is much more difficult to design a supported catalyst with larger particles (i.e. more than 1 nm in diameter) keeping a monomodal particle size distribution. Post treatments, such as drying, calcinations, and reduction steps under different atmospheres (wet, reductive, and oxidative) have also been widely studied in order to control sintering and ultimately the characteristics of the supported particles.[16,17] Using thermal sintering, even under optimized conditions, it is very difficult to obtain a monomodal particle size distribution or a homogeneous composition along with a controlled metal–support interaction.

Various catalytic reactions are known to be structure sensitive as proposed by Boudart[6] and studied by many authors.[7–9] Examples are the selective hydrogenation of polyunsaturated hydrocarbons, hydrogenolysis of paraffins, and ammonia or Fischer–Tropsch synthesis. Controlled surface reactions such as oxidation–reduction reactions[10–13] or surface organometallic chemistry (SOMC)[14,15] are two suitable methods for the synthesis of mono- or bimetallic particles. However, for these techniques, the redox potential and the availability or reactivity of the organometallic precursors may be a limitation for some elements.

Concerning catalytic applications, such as selective hydrogenation of polyunsaturated hydrocarbons, an eggshell repartition of the active phase is often required for mass-transfer considerations, combined to a well-defined particle size (around 20 to 50 Å depending on the substrate) because of the aforementioned structure sensitive phenomena. Furthermore, most of the catalysts designed for these applications contain more than one element and obviously an association at a nanometer scale of the principal element to the promoter is targeted. All these characteristics involve a very high level of control, which is quite difficult to achieve mainly if aqueous and one-pot synthesis is required for environmental, economic, and scaling up considerations. In this area, colloidal oxide synthesis also appears to be an alternative route able to meet the requirements of the most sophisticated supported catalysts produced in industrial manufacturing processes. The scientific bases of this method have been extensively studied and applied for a long time in the synthesis of new oxide solids that are well-defined in terms of size, crystalline structure, and morphology.[18,19] As an example, it has been successfully applied to the synthesis of various metal oxides ($\alpha-Fe_2O_3$, β-FeOOH, Co_3O_4, ZrO_2, Cr_2O_3, ZnO).[20] Less attention has been given to the last series group VIII metals, and more particularly, to the noble metals used in catalysis for refining and petrochemical applications. Synthesis of metallic colloidal nanoparticles has been identified as a powerful preparation method in order to prepare mono- and bimetallic supported catalysts. Nucleation of reduced atoms activated by various methods (photoreduction, radiolysis, or chemical reduction) produces well-calibrated particles, which can be further deposited on different supports.[21–23] These studies have demonstrated the great interest to control the parameters related to the particles such as size, distribution, and morphology.[24] However, most of the work deals with organic solutions and colloidal particles generated via a chemical, radiolytic, or reduction process. In spite of the obvious advantages of using aqueous instead of organic solutions, due to safety and economic aspects, the synthesis of supported metal catalysts from oxide colloidal suspensions has not until recently received significant attention. Moreover, all options offered by the sol–gel chemistry have not yet been entirely explored to produce designed supported nanoparticles.

Unlike most of the industrial preparation methods, colloidal oxide synthesis does not make use of the chemistry between metallic ions in solution and the surface sites of the oxide carrier (hydroxyl or Lewis acid sites). Indeed, the strategy disconnects the steps corresponding to the formation of particles, synthesized previously in solution, and to the subsequent deposition and activation on the oxide carrier.

Covering monometallic (Pd, Sn) and multimetallic (Pd–Sn, Pd–Ag) systems, several examples are presented in this chapter to illustrate the possibility offered by this chemistry to control the particle size distribution and the bimetallic interaction at a molecular level. This work is supported by a multitechnique characterization approach using: ^{119}Sn Mössbauer spectroscopy, X-ray photoelectron spectroscopy (XPS), low-energy ion spectroscopy (LEIS), and transmission electron microscopy (TEM). Catalytic performances in hydrogenation of different unsaturated hydrocarbons (phenylacetylene, butadiene) are finally discussed in order to establish structure–reactivity relationships.

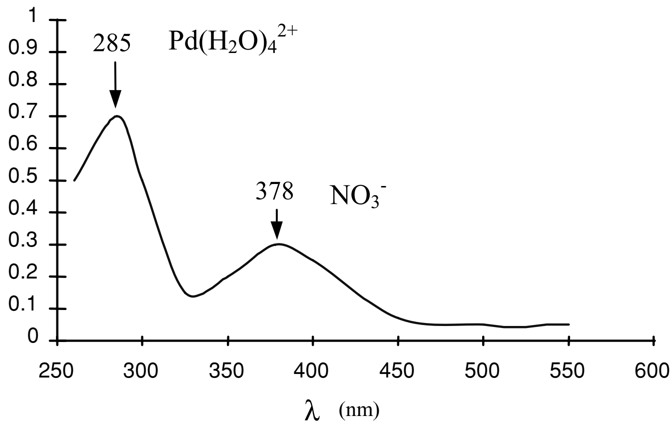

FIGURE 13.2. UV–visible spectrum of the initial $Pd(NO_3)_2$.

13.2. SYNTHESIS OF MONOMETALLIC CATALYSTS

13.2.1. Synthesis of Palladium Oxide Hydrosols

Oxide hydrosols synthesis relies on the destabilization of a true solution by a pH change. In order to prepare palladium oxide colloidal particles, two experimental routes can be carried out: the neutralization of an acidic (basic) solution by an alkaline (acidic) solution, or thermohydrolysis of the palladium precursor solution.

The different molecular species present in a palladium nitrate solution can be easily identified by UV–visible spectroscopy (Fig. 13.2). Two absorption peaks are generally observed at $\lambda = 285$ nm and $\lambda = 378$ nm, the latter being ascribed to free nitrate ions corresponding to the electronic transition from the σ to the π^* state in the NO_3^- ions, as observed in the case of an aqueous solution of $NaNO_3$. The other absorption band at $\lambda = 285$ nm is assigned to a d–d transition in the aquo complex $Pd(H_2O)_4^{2+}$.[26] These UV–visible results show the noncomplexant behavior of nitrate ions toward palladium metallic centers. The palladium containing species in the starting solution is then the planar tetra-aquo complex $Pd(H_2O)_4^{2+}$.

The water molecule in the Pd cationic complex $Pd(H_2O)_4^{2+}$ brings an electric charge of $+0.37$, calculated according to the partial charge model as described by Jolivet and Hiemstra et al.[27,28] This positive charge indicates that the aquo ligand has an electrophilic character. As a consequence, condensation of aquo cationic complexes cannot occur spontaneously. The charge calculation is thus in agreement with UV–visible results which show monomolecular stable Pd species in the acidic solution.

The formation of palladium oxide colloidal particles from an acidic palladium nitrate solution can be achieved by addition of an alkaline solution. The different steps, describing the chemistry involved in such a process are[29]

– nucleophilic attack of hydroxyl ions leading to the substitution of hydroxo ligands and formation of a complex with no electric charge: $Pd(OH)_2(H_2O)_2$,

TABLE 13.1. Partial charge of the hydroxo ligand and metallic center for different metallic precursors.

Metallic Salts	Complex in Solution	Corresponding Hydroxyl Complex	δ(Pd)	$\delta(H_2O)$	δ(OH)
$Pd(NO_3)_2$	$Pd(H_2O)_4{}^{2+}$		0.49	0.37	
		$Pd(OH)(H_2O)^+$	0.46		0.00
		$Pd(OH)_2(H_2O)_2$	0.35		−0.19
Na_2PdCl_4	$PdCl_3(H_2O)^-$		0.19	−039	
	$PdCl_3(OH)^{2-}$		0.01		−0.75
		$Pd(H_2O)_2Cl\ (OH)$	0.34		−0.19
$K_2Pd(NO_2)_4$	$Pd(NO_2)_4{}^{2-}$	$Pd(NO_2)OH(H_2O)$	0.43		−0.05
$Pd(NH_3)_4(NO_3)_2$	$Pd(NH_3)_4{}^{2+}$	$Pd(NH_3)_2(OH)_2$	0.29		−0.29

– inorganic polymerization or condensation by olation reactions between these complexes and formation of nuclei, and
– growth of these nuclei by olation reactions.

In the case of the $Pd(OH)_2(H_2O)_2$ complex, the partial charge model predicts condensation because of the nucleophilic character of the hydroxo ligand toward the metallic center (Table 13.1). The partial charge of the nucleophilic group ($\delta_{OH} = -0.19$) and the electrophilic center ($\delta_{Pd} = +0.35$) meet the R. Anderson principle ($\delta_{OH} < 0$ and $\delta_{Pd} > +0.3$). This criterion is not filled for every molecular precursor (for ex. $Pd(NH_3)_4(NO_3)_2$, $K_2Pd(NO_2)_4$) depending on the stabilization effect of the ligand.

Finally, PdO particles are spontaneously formed from palladium hydroxide $Pd(OH)_2$ via dehydration by internal oxolation in agreement with the positive value of the partial charge of the water molecule ($\delta_{H2O} = 0.03$). Figure 13.3 summarizes the overall mechanism leading to the formation of PdO colloidal particles.

Figure 13.4 shows the titration curve of a palladium nitrate solution [Pd] = 5 g/L by soda [NaOH] = 0.1 N. Three regions can be clearly distinguished, corresponding to a true solution (starting point until addition of about 14 mL of soda), to the formation of colloidal PdO particles (from 14 to 24 mL added), and to the flocculation of particles with segregation of liquid and solid phases (above 25 mL).

The preparation of colloidal particles can be performed by the addition of a well-defined amount of soda corresponding to the second intermediate zone. The neutralization process corresponds to simultaneous titrations of free acidity brought by nitric acid and a palladium complex according to the following reactions:

$$HNO_3 + NaOH \rightarrow NaNO_3 + H_2O \tag{1}$$

$$Pd(H_2O)_4{}^{2+} + 2\,NO_3{}^- + 2\,NaOH \rightarrow 2\,NaNO_3 + Pd(OH)_{2+}4\,H_2O. \tag{2}$$

It is worth noticing that for pH > 2, reaction (2) is complete as shown by the absence of the molecular complex $Pd(H_2O)_4{}^{2+}$ in the solution analyzed by UV–visible spectroscopy. X-ray diffraction diagrams of dried suspensions after neutralization confirm

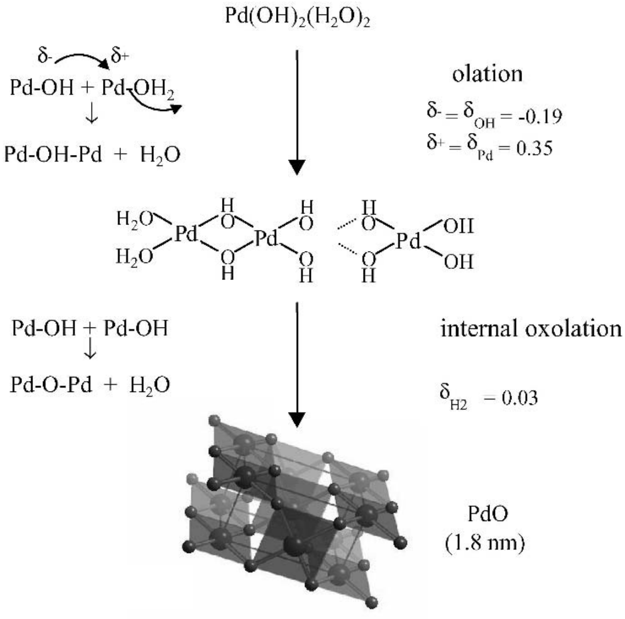

FIGURE 13.3. Reaction mechanisms involved during the synthesis of PdO colloidal particles from palladium hydroxo complexes.

the exclusive formation of palladium oxide identified by comparisons to the JCPDS database (Fig. 13.5).

Using the multisite complexation model (MUSIC),[30] the surface of palladium oxide has been modeled providing useful data on the nature, number, and the acid–base strength of the hydroxyl groups present on the different faces (1 1 1) and (1 0 0) of

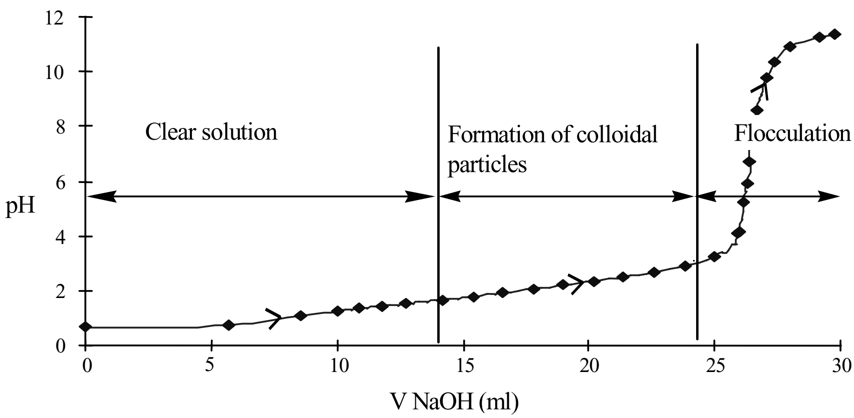

FIGURE 13.4. Neutralization curve of a palladium nitrate solution [Pd] = 5 g/L by addition of soda [NaOH] = 0.1 N.

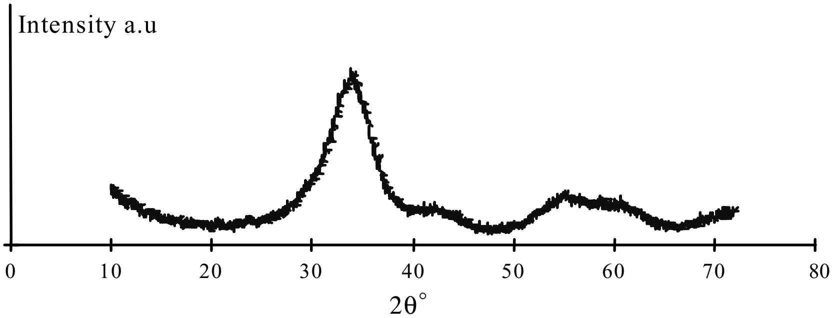

FIGURE 13.5. X-ray diffraction pattern of dried suspension after neutralization by soda.

the PdO crystal (Fig. 13.6). One can see the good agreement between the value of the isoelectric point given by this model and the value of 4.5 determined experimentally by the potentiometric titration method described in Ref. 31.

Particle size distributions of both hydrosols determined using a statistical image analysis of transmission electron microscopy (Jeol TEM 120 CX) micrographs are presented in Fig. 13.7. These hydrosols were prepared at different neutralization levels (pH = 2 and 2.8). Both particle size distributions are centered around 18 to 19 Å and are extremely sharp as shown by the low values of the standard deviation σ.

The reverse operation, i.e. the addition of palladium nitrate solution to soda, can also be used to prepare colloidal suspensions. Figure 13.8 presents the corresponding titration curve of a soda ([NaOH] = 0.2 N) by a palladium nitrate solution ([Pd] = 5 g/L).

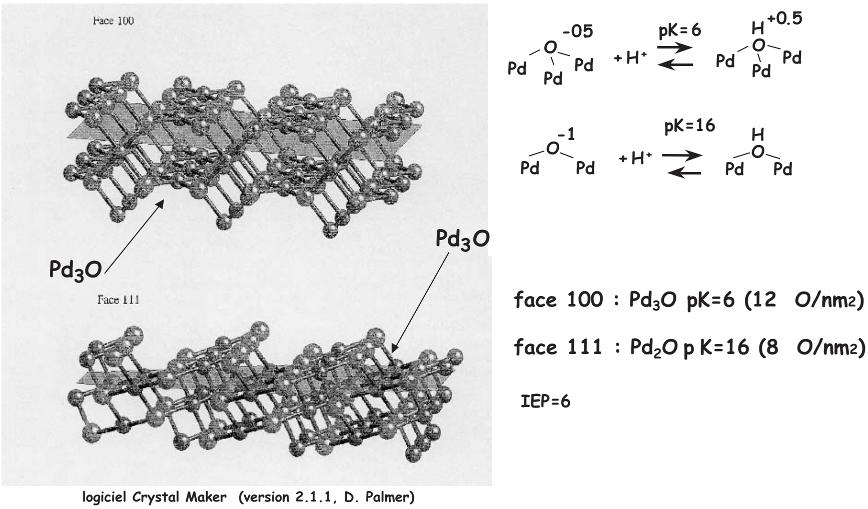

FIGURE 13.6. Molecular modeling of the surfaces of PdO (111) and PdO (100) by CristalMaker. Calculation made by J. Hernandez and C. Froidefond (LCMC, UPMC PARIS VI).

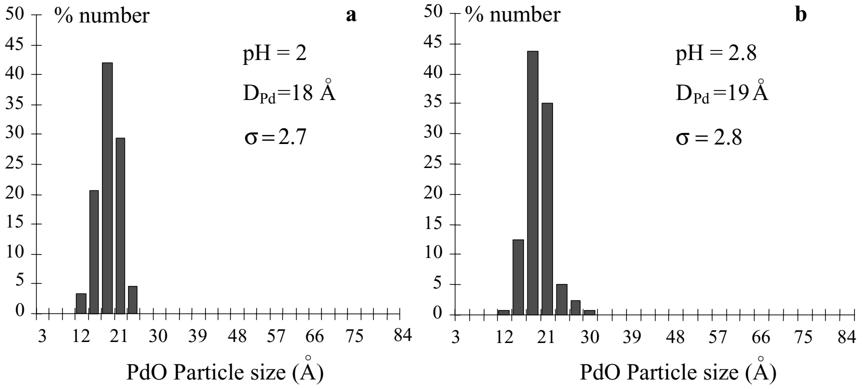

FIGURE 13.7. PdO particle size distributions obtained by neutralization of palladium nitrate solution by soda at different pH determined by transmission electron microscopy.

Particle size distributions obtained via direct (pH = 1.8) or reverse procedure (pH = 12) are very narrow and both centered around 17 to 18 Å (Fig. 13.9).

Micrographs of replica (Fig. 13.10) obtained by vitrification in liquid propane (performed at the biology laboratory IFR 2062, Paris VI University, F. Gaill.) reveals the presence of large three-dimensional aggregates for the hydrosol prepared in basic pH (12.3).

For the formation of the different species (oxides or hydroxylated), one must take into account both kinetic and thermodynamic aspects. In Fig. 13.11, one can see that despite the stable character predicted by the thermodynamic diagram (Fig. 13.12) of the $Pd(OH)_2(H_2O)_2$ at pH = 12.6, only $Pd(OH)_4{}^{2-}$ (band at 368 nm[32]) is formed in the previous stage of the synthesis. This complex is slowly converted into $Pd(OH)_2$ and then into PdO after a few minutes as shown by the disappearance of the absorption band of the $Pd(OH)_4{}^{2-}$ complex.

For catalytic purposes, it is generally important to optimize the exposed surface area of active sites, and as a consequence one must control the degree of aggregation of the colloidal particles. These suspensions are metastable thermodynamic systems

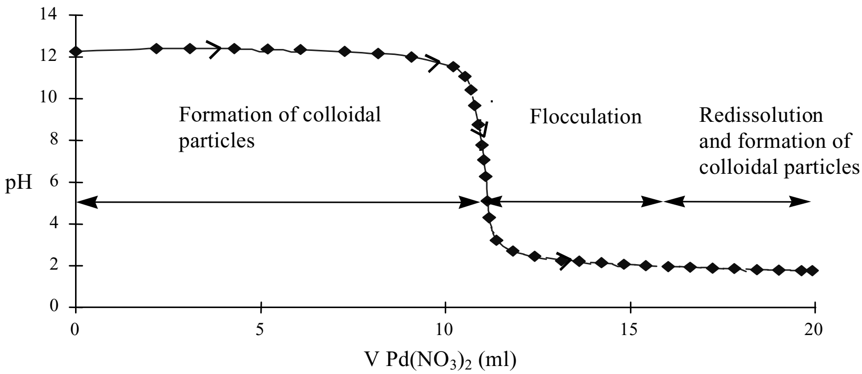

FIGURE 13.8. Neutralization curve of soda [NaOH] = 0.1 N by addition of a palladium nitrate solution [Pd] = 5 g/L.

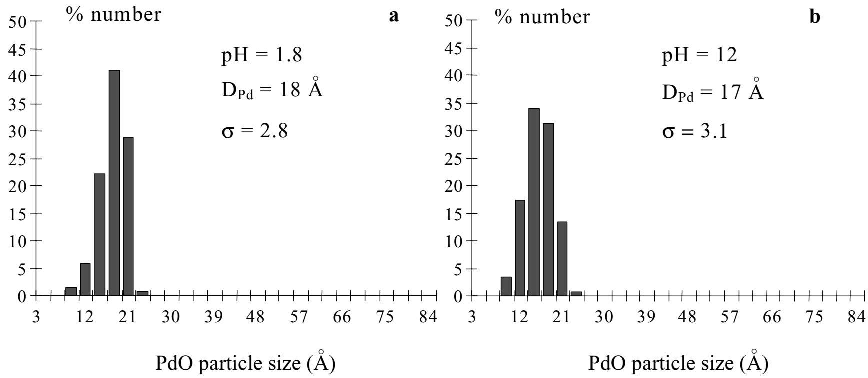

FIGURE 13.9. PdO particle size distributions for different pH by neutralization of palladium nitrate by soda (a) and soda by palladium nitrate (b) as determined by TEM.

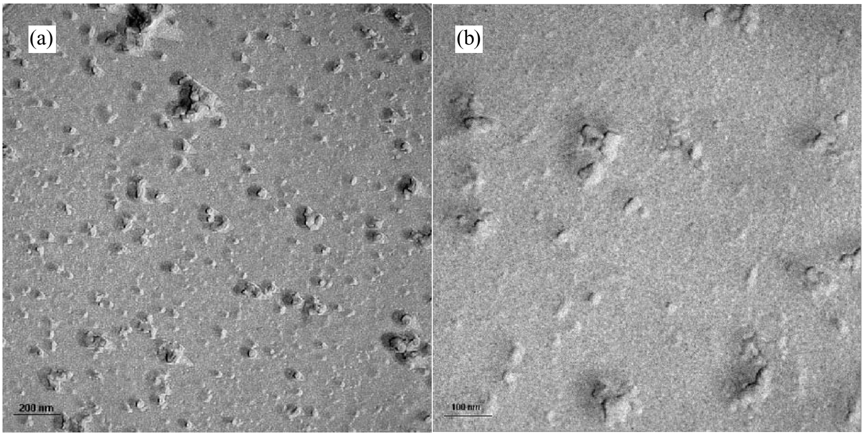

FIGURE 13.10. Micrographs after vitrification in liquid C_3H_8 of a basic hydrosol.

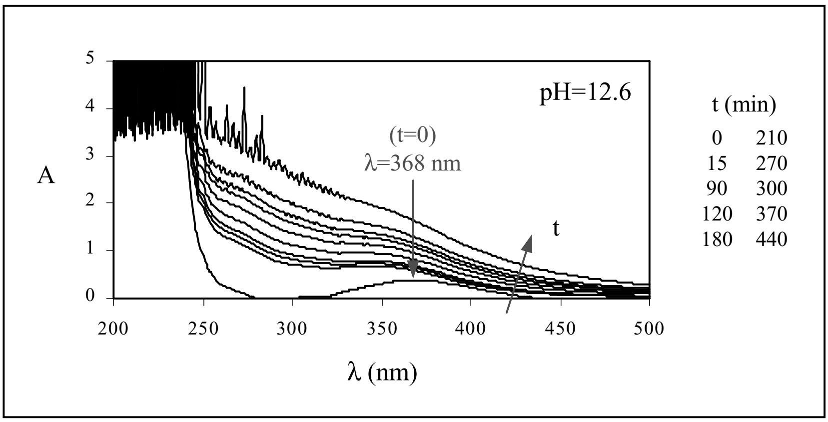

FIGURE 13.11. UV–visible spectra of the SB PdO hydrosol (pH = 12.6) ([Pd] = 3.40 g/L) versus time.

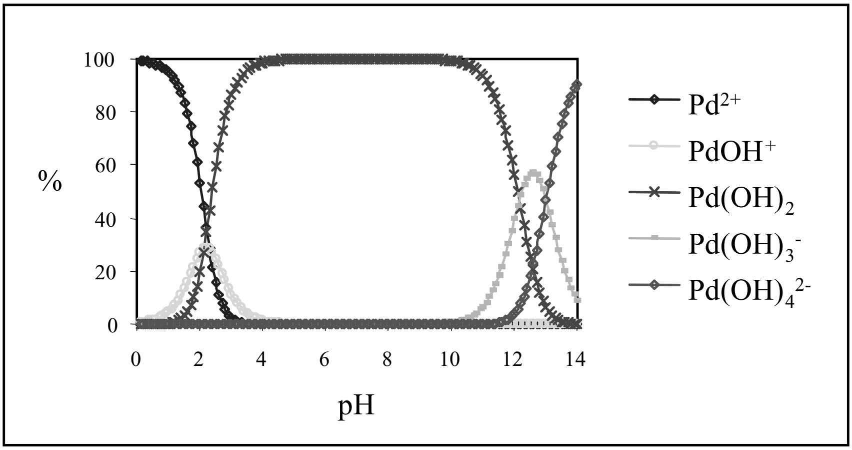

FIGURE 13.12. Stable existing species as a function of pH ([Pd] = 10 g/L = 9.4×10^{-2} M and I = 1 M) from Ref. 35.

and various operating parameters have a strong influence on the physical stability of the sol: ionic strength, addition of a stabilizing agent (surfactant, polymers, complexant), the pH of the medium, and temperature. Aggregation phenomena (or desaggregation which is generally the objective for catalytic applications), are closely related to the solubility of the oxide phase in the medium. Experimental data clearly shows that isolated particles are more easily obtained for pH conditions where solubility of the oxide solid phase is not zero. On the other hand, aggregation is more favored when solubility of the solid phase is very low. As an example, isolated PdO particles can be obtained for an acidic pH (for example with a reacidification at pH < 2), whereas highly aggregated PdO particles are observed for basic pH (typically pH > 12), resulting in a low solubility of PdO. In this case, physical phenomena like electrostatic interaction seem to play a minor role with respect to chemical solubility. Variations of $|\text{pH-PIE}_{\text{PdO}}|$, which is the driving force for the repulsive interaction between particles (2.5 for the acidic medium when pH = 2, and 7.5 in basic medium when pH = 12), and the ionic strength values are not able to explain the aggregation–desaggregation process.

The same results were observed for other oxide-colloidal systems such as SnO, SnO_2, and NiO. It is interesting to note that this tendency seems to be a general feature of oxides in solution as it has been observed for other systems.[33,34] Using the quasielastic light scattering (QELS) technique (Fig. 13.13), it is possible to follow the size of the PdO aggregates in the colloidal suspensions, while changing the operating conditions (in this case, the pH, but the concentration of Pd and time could be varied as well).

We have seen that direct and reverse neutralization lead to the same average particle size. In order to explain this result, one must consider the chemical reactions occurring during both preparations. Although several monomolecular species are thermodynamically predicted (Fig. 13.12), the determination of the partial charge of the hydroxo ligand in different complexes shows that this ligand is the only one exhibiting

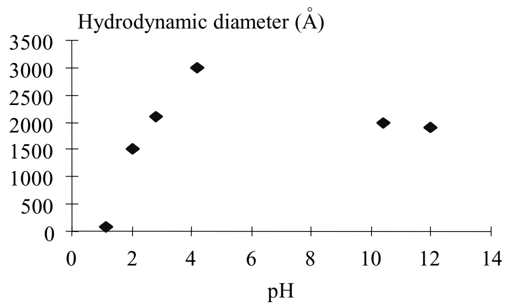

FIGURE 13.13. Hydrodynamic diameters of colloidal particles determined by QELS as a function of the hydrosol pH.

the nucleophilic character necessary for the condensation mechanism (Table 13.1). For pH < 12, the anionic species $Pd(H_2O)(OH)_3{}^-$ and $Pd(OH)_4{}^{2-}$ are not present. Thus, both types of neutralization, addition of soda to nitric acid and the reverse, lead to the same complex, i.e. $Pd(H_2O)_2(OH)_2$ which is the only complex able to generate nuclei by polycondensation. It has been verified by UV–visible measurements that for pH < 12, no molecular complex was observed.

For direct neutralization (addition of soda into palladium nitrate) different hydrolyzed intermediate species can be formed from $Pd(H_2O)_4{}^{2+}$ (Fig. 13.14): $Pd(H_2O)_2(OH)_2$, $Pd(H_2O)_3(OH)^+$. In the reverse method, i.e. the addition of $Pd(H_2O)_4{}^{2+}$ in a NaOH solution at pH $= 12$, the only complex produced is the neutral complex $Pd(H_2O)_2(OH)_2$, in agreement with UV–visible measurements. In this case, the cloudy solution appears in the initial stage of the experiment with the first drops of palladium nitrate solution.

Moreover, the formation of $Pd(H_2O)_2(OH)_2$ by substitution of aquo groups by hydroxo groups is very fast ($k = 10^{10}$ mol^{-1} s^{-1}), and as a consequence, the concentration

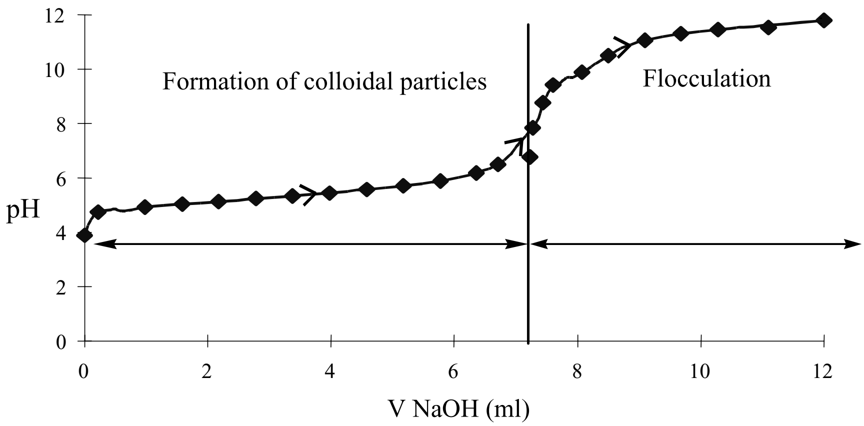

FIGURE 13.14. Neutralization curve of a palladium chloride solution [Pd] = 5 g/L by addition of soda [NaOH] = 0.1 N.

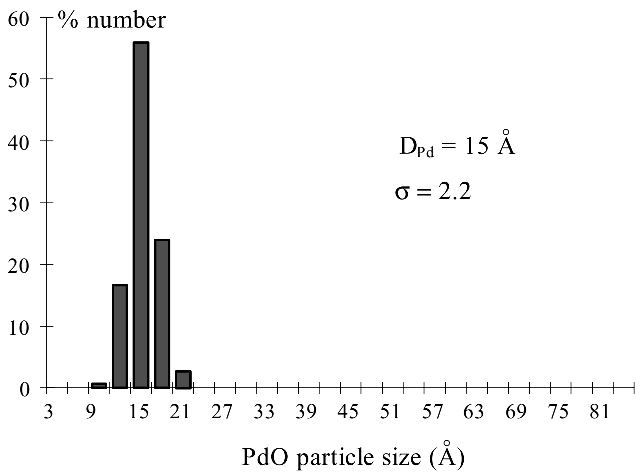

FIGURE 13.15. PdO particle size distributions obtained by neutralization at pH = 7 of Na_2PdCl_4 solution by soda determined by transmission electron microscopy.

of this complex is very high for all preparations. This fast reaction is responsible for the high sursaturation values defined by the ratio of the concentration of metallic precursor $Pd(H_2O)_2(OH)_2$ in the solution to the solubility of the solid PdO phase. At room temperature and solutions with a pH ranging from 3 to 12, high sursaturation values are reached as well due to the very low value of the pKs of the solid precursor ($\sim 1.1 \times 10^{-29}$). This high value of sursaturation favors the nucleation rate with respect to the growth rate from a kinetic point of view. This "explosive" nucleation step governs the final PdO particle size. In the case of the Pd nitrate precursor, no growth above a size of about 2 nm of the particles has been achieved varying the other operating parameters of pH, ionic strength, nature of the counter ion of hydroxides, or metal concentration.

One way to modify the final particle size is to generate a different precursor of condensation. As an example, Na_2PdCl_4 in acidic solution contains the $PdCl_3(H_2O)^-$ complex as seen by UV–visible measurements. Neutralization by soda leads to the formation of two types of neutral complexes: $Pd(H_2O)_2ClOH$ and $Pd(H_2O)_2(OH)_2$. According to the partial charge model, these two complexes are able to polymerize ($\delta_{OH} = -0.19$ and $\delta_{Pd} = +0.34$ in the case of $Pd(H_2O)_2ClOH$ complex, Table 13.1). By inductive effect, the chloride ligand affects the kinetics of the nucleation rate versus growth of the entities. As a result, the final particle size is slightly lower than compared to the results obtained starting with palladium nitrate solution (Fig. 13.15).

This effect, moderated by the presence of $Pd(H_2O)_2(OH)_2$, is clearly related to the properties of the $Pd(H_2O)_2ClOH$ complex. The reverse neutralization (addition of Na_2PdCl_4 or $PdCl_3(H_2O)^-$ under its hydrolyzed form, to soda) gives rise only to $Pd(H_2O)_2(OH)_2$ formation due to the instability of $PdCl_3(H_2O)^-$ at high pH values.[36] For these conditions, the consecutive condensation reactions generate palladium oxide particles with the same average size as in preparations using palladium nitrate precursor.

Thermohydrolysis is another reaction which can be used to prepare colloidal suspensions of palladium oxide particles, and has been proven for other oxides.[37–40]

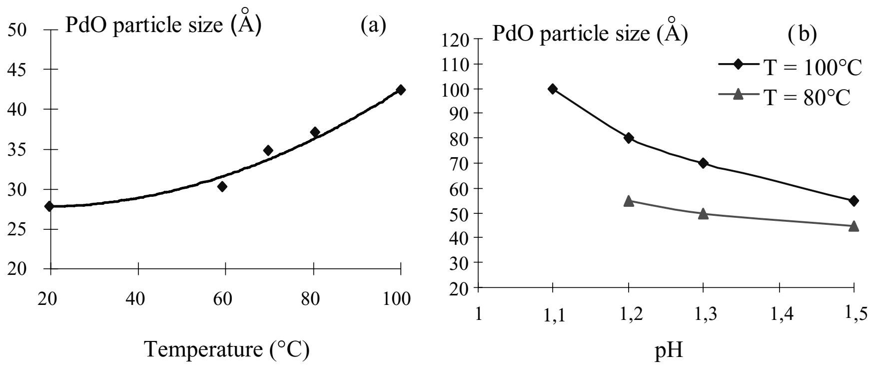

FIGURE 13.16. Evolution of PdO particle size with temperature and pH (a: starting $Pd(NO_3)_2$ solution [Pd] = 5 g/L and b: [Pd] = 1 g/L).

In this case, the reaction of water molecules with palladium complexes is promoted by heat, so no addition of soda is required. The global chemical reaction is expressed by Eq. (3):

$$[Pd(OH_2)_4]^{2+} + 2NO_3{}^- + hH_2O \rightarrow [Pd(OH)_h(OH_2)_{4-h}]^{(2-h)+} + 2NO_3{}^- + hH_3O^+. \quad (3)$$

In comparison with the neutralization methods previously described, lower sursaturations are obtained with thermohydrolysis because the solubility of $Pd(H_2O)_2(OH)_2$ increases with temperature. Thermohydrolysis is then more favorable to particle growth. Figures 16a and b present the influence of temperature and the initial pH of the solution on the average PdO particle size determined by X-ray diffraction on the solid phase after precipitation.

PdO particle growth may have two origins: A thermodynamic phenomenon due to the spontaneous evolution in order to minimize surface energy of the system by Ostwald ripening, or a kinetic control of nucleation and condensation reaction rates. In our case, no variation of the final particle size was observed between the first 18 h at 100°C under reflux. So, the evolution of average particle size is probably more related to a kinetic effect. Lowering the pH displaces the equilibrated reaction (3) to the left, depressing the formation of the neutral precursor $Pd(H_2O)_2(OH)_2$ ($h = 2$). Moreover, at low pH values, the solubility of PdO oxide is enhanced, decreasing the sursaturation of the medium. The nucleation rate, which is greatly dependent on the concentration of the nuclei, is then lower and the nuclei are less numerous and may grow by condensation reactions. The effect of temperature may also be explained in terms of kinetic control of the formation of solid nuclei, increasing their solubility and lowering the sursaturation of the solution.

13.2.2. Synthesis of Tin Oxide Hydrosols

Using the same experimental procedure as previously described, destabilization of a chloride stannic ($SnCl_4$, $5H_2O$) solution by the addition of soda easily forms a colloidal suspension. Figure 13.17 presents a TEM micrograph of a colloidal SnO_2

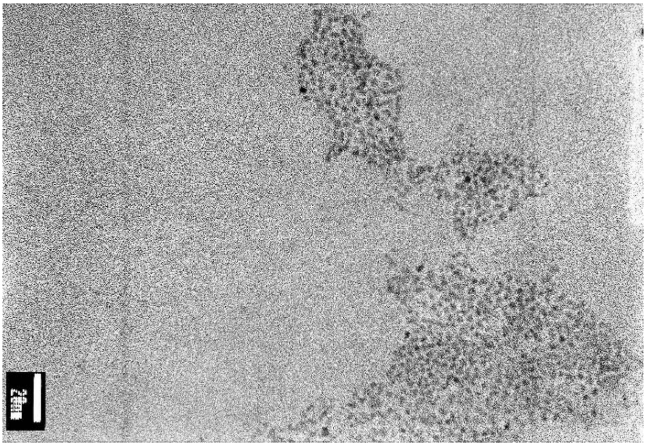

FIGURE 13.17. TEM micrograph of SnO_2 hydrosol (pH = 0.5) diluted 100 times with water.

(pH = 0.5) suspension deposited on a grid. Monomodal particle size distributions are obtained with an average size close to 2 nm.

The X-ray diffraction pattern of the solid phase obtained by complete neutralization of an acidic solution of $SnCl_4{\cdot}5H_2O$ is presented in Fig. 13.18. Cassiterite SnO_2 (rutile-type structure) was identified and Laue–Scherrer's law gives an average particle size of 2 ± 0.2 nm in good agreement with transmission electron microscopy observations.

Figure 13.19 summarizes the reaction mechanism starting from $Sn(OH)^{3+}$ or $Sn(OH)_6{}^{2-}$ in acidic media in alkaline media. As in the case of Pd, SnO_2 oxide is spontaneously formed by dehydration due to an internal oxolation reaction promoted by a strong polarization of the O–H bond of the hydroxide. Thermodynamically stable species with respect to pH are presented in Fig. 13.20. Various molecular cationic species with different hydroxylated levels are possible in an acidic medium, whereas only $Sn(OH)_6{}^{2-}$ is expected for a basic pH.

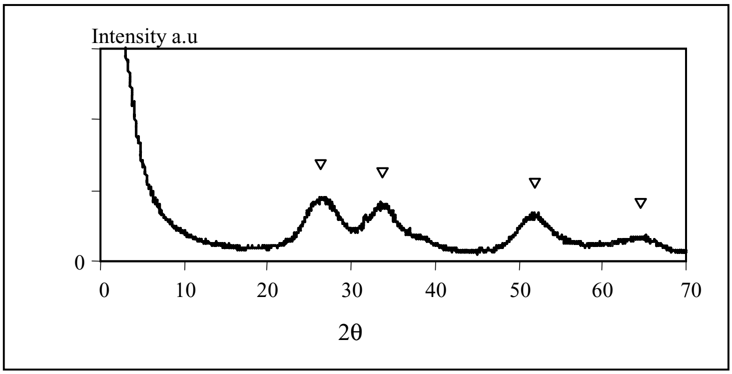

FIGURE 13.18. X-ray diffraction diffractogramm of the solid phase obtained by complete neutralization of a $SnCl_4{\cdot}5H_2O$ acid solution ∇SnO_2.

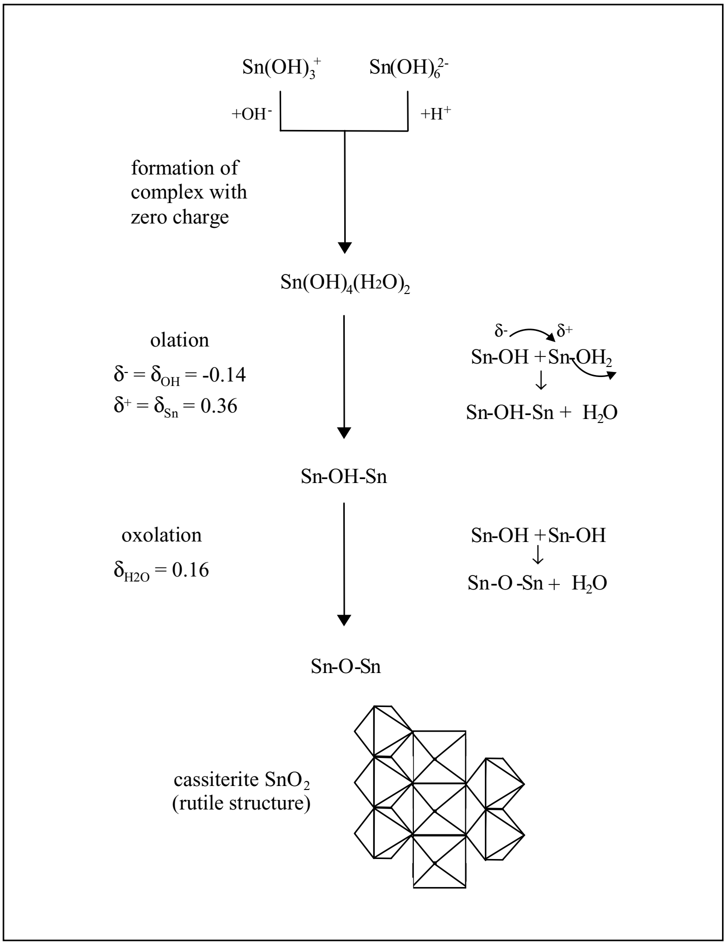

FIGURE 13.19. Schematic mechanism of the formation of SnO_2 (Cassiterite).

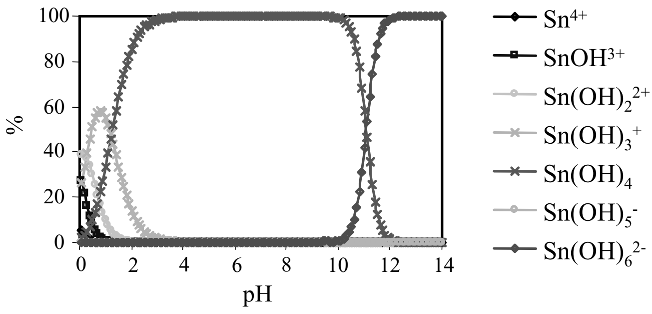

FIGURE 13.20. Repartition diagram of Sn^{IV} species ([Sn] = 10 g/L and I = 1 M).

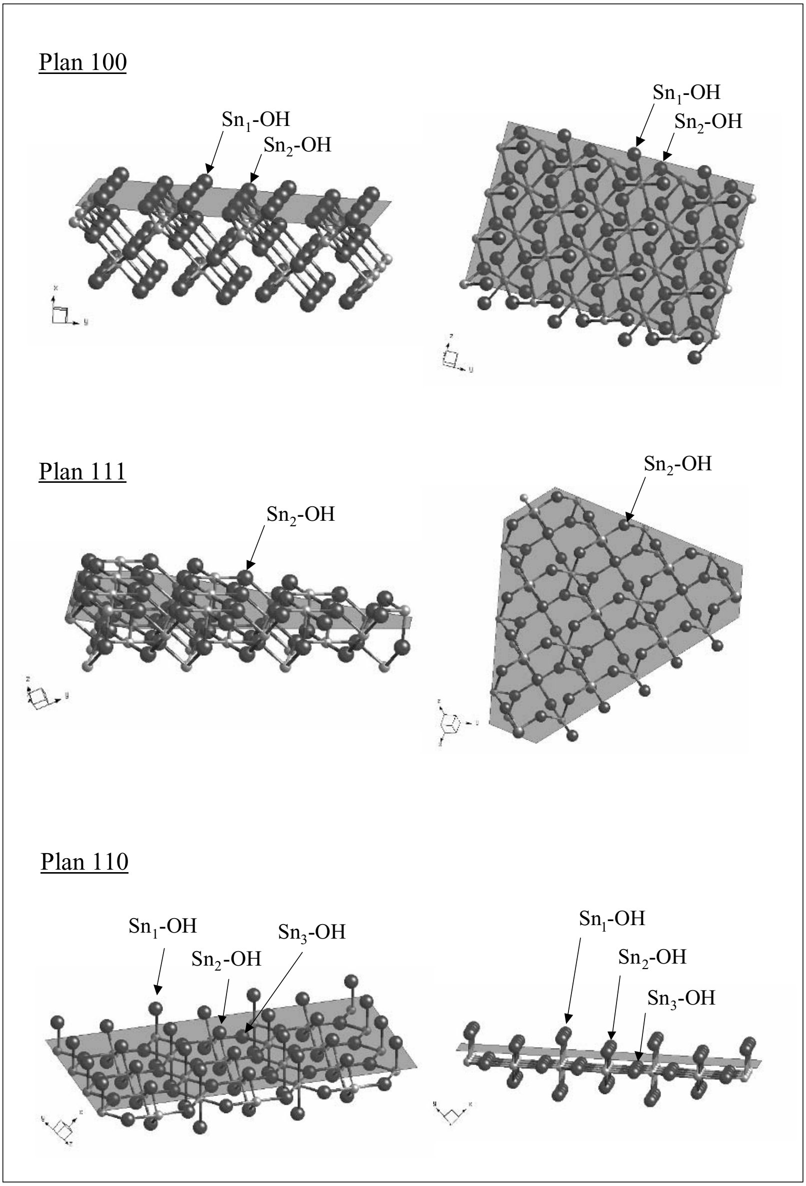

FIGURE 13.21. Surface sites of SnO_2 crystal (cassiterite) obtained with CrystalMaker 2.1.1 software.

The surface structure and characteristics (density and acidity) of the hydroxyl groups presented in Fig. 13.21 (using CrystalMaker 2.1.1 software) give very useful information to understand the reactivity of the surface of the particles, particularly when adsorption of another complex is desired to synthesize a bimetallic catalyst, or to control the interaction with an oxide carrier (the deposition step). The isoelectric point calculated with the model (5.9) is in fair agreement with the experimental value (4.3).

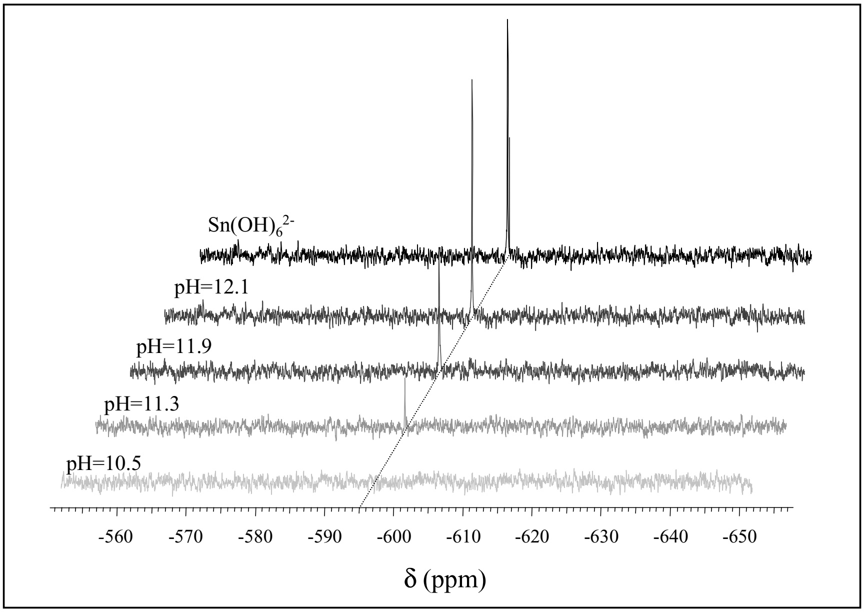

FIGURE 13.22. ^{119}Sn NMR spectra of hydrosol of SnO_2 and of the solution $Sn(OH)_6{}^{2-}$ ([Sn] = 3.67 g/L).

Using ^{119}Sn NMR spectroscopy, it is possible to follow the dissolution of SnO_2 and the formation of $Sn(OH)_6{}^{2-}$ (Fig. 13.22). During the hour long preparation, this complex is formed for pH $>$ 11.3 (signal at 595 ppm) in agreement with the thermodynamic diagram in Fig. 13.20. The optimal OH/metal ratio must be determined to neutralize all the initial precursors without promoting dissolution.

13.2.3. Alumina-Supported Palladium Catalyst

The colloidal suspensions obtained by the neutralization or thermohydrolysis procedures described previously have been used to prepare supported Pd catalysts. The support is impregnated with a volume of colloidal oxide suspension corresponding exactly to the porous volume of the solid, according the well-known incipient wetness impregnation.

Various supports have been used, but the results reported here have been exclusively obtained with δ-Al_2O_3 with a specific surface area of 130 m^2/g and a porous volume of 1.04 cm^3/g. The palladium loading is about 0.1% by weight. After impregnation, the samples are dried overnight at 393 K.

Figures 13.23a and b show the PdO particle size distribution of PdO-supported catalysts prepared from an acidic hydrosol (neutralization of palladium nitrate solution by addition of soda) and a basic one (neutralization of soda by addition of palladium nitrate). Comparisons with the corresponding histograms of the initial suspensions (Figs. 7b and 9b), show that the distributions are not significantly modified. Only a very slight increase of the standard deviation of the dispersion values is observed

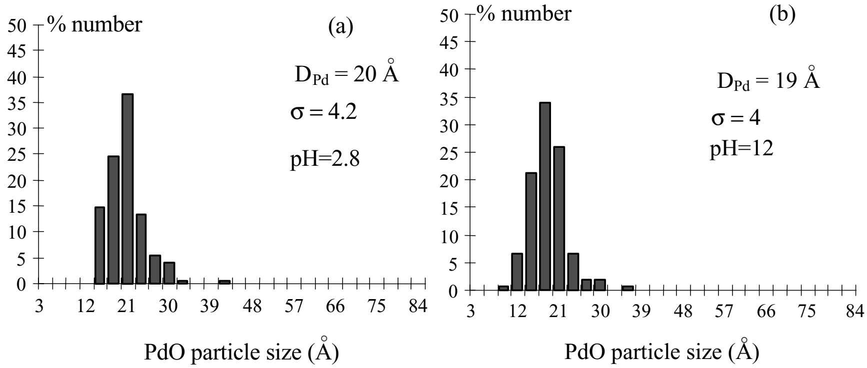

FIGURE 13.23. PdO particle size distributions for samples prepared from an acidic hydrosol pH = 2.8 (a) and a basic one pH = 12 (b).

($\sigma = 4$ to 4.2 instead of $\sigma = 2$ to 3 for hydrosols), with the same average sizes of PdO particles.

Transmission electron microscopy micrographs (Fig. 13.24) also indicate an important characteristic of the supported particles. As in the case of suspensions, they are either aggregated or isolated. Support surface properties may be an important factor governing this aggregation. After deposition on the support, we observed that samples prepared from acidic hydrosols are characterized by the presence of aggregated particles constituting flocculates ranging from 10 to 200 nm, whereas samples prepared via basic hydrosols contain only isolated particles. The opposite was observed when hydrosols were concerned. These final states of the supported particles may be controlled

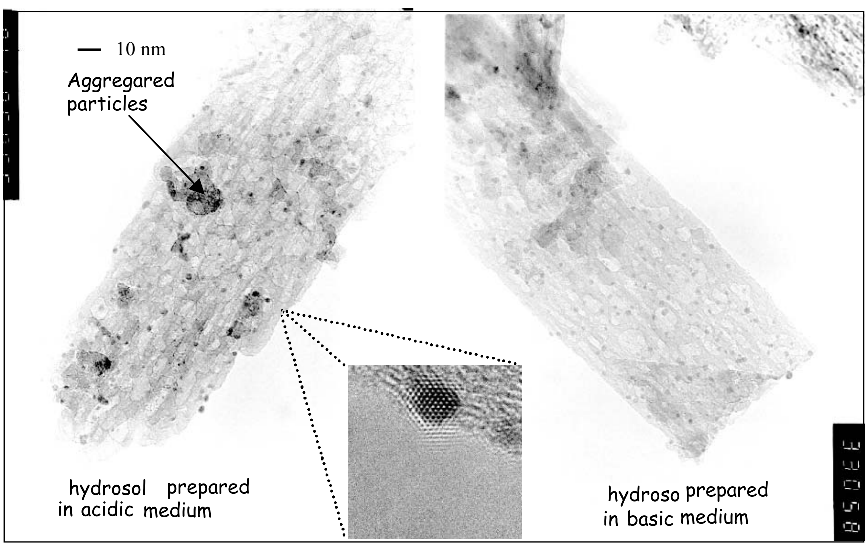

FIGURE 13.24. TEM micrographs of supported PdO catalysts prepared via "acid" and "basic" hydrosols.

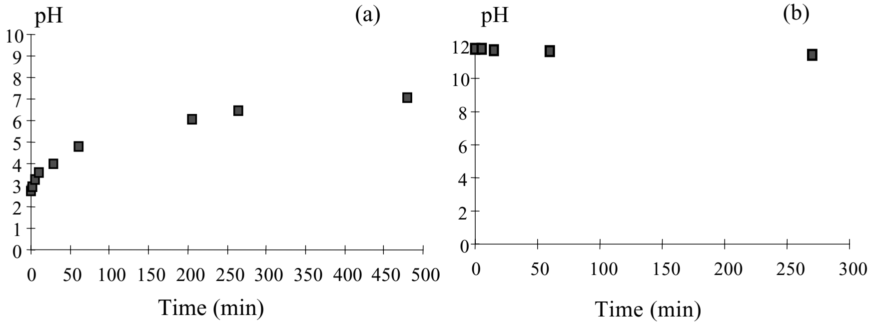

FIGURE 13.25. Evolution of pH of an acidic suspension (a: pH = 2.8) and basic suspension (b: pH = 12) in contact with δ-Al_2O_3.

via the pH of the suspension and its adequation with the isoelectric point of the solids (PdO particles and support), or the addition of a dispersing agent in the hydrosol before the impregnation step.

In the case of the impregnation of the acidic hydrosol (pH = 2.8), the surface of alumina is positively charged and the protonation of the surface hydroxyl groups is rather slow but significant when compared to the duration of preparation (around 30 min). After 200 min, the equilibrium is reached at a pH of approximately 7 (Fig. 13.25a). Keeping in mind that the IEP value of the palladium oxide is 4.5 in these conditions, both the support and PdO particles are initially positively charged and have a repulsive interaction favoring an isolated state at pH = 2.8. The progressive increase of pH due to the alumina protonation destabilizes the PdO particles repulsion leading to aggregated particles.

Impregnating a basic colloidal suspension (pH = 12) on alumina does not induce proton liberation, thus the pH is constant (Fig. 13.25b). The system keeps its initial properties, i.e. negative charges for alumina support and PdO particles. Repulsive interactions are created between the alumina surface and the PdO particles so that the particles deposited on the support are redispersed, and finally isolated from each other.

The aggregation state of particles can also be controlled by addition of dispersing agents to the hydrosol. As shown by transmission electron microscopy, samples stabilized by nitrite or chloride anions contain isolated particles for a very long period. The oxide particles, stabilized by the formation of Pd–NO_2 bonds, are isolated in the hydrosol. Because this bond is stable at the high pH values obtained during the deposition on alumina, the isolated state is retained for the final PdO supported catalyst. Since the stabilization by a strong ligand may also lead to redissolution of palladium oxide particles, one must precisely adjust the quantity of stabilizing agent. The use of steric stabilization may also be successfully employed with a cationic surfactant such as cethyl triammonium bromide (CTAB).

Reduction of PdO particles to metallic Pd° does not significantly modify the size of the particle to the extent shown by the BIOSYM calculation (Fig. 13.26). This important result means that the optimization of the size of the PdO particle, carried out during the preparation of the suspension, should remain even after activation, i.e. reduction under hydrogen, necessary for catalytic purposes to produce metallic active sites.

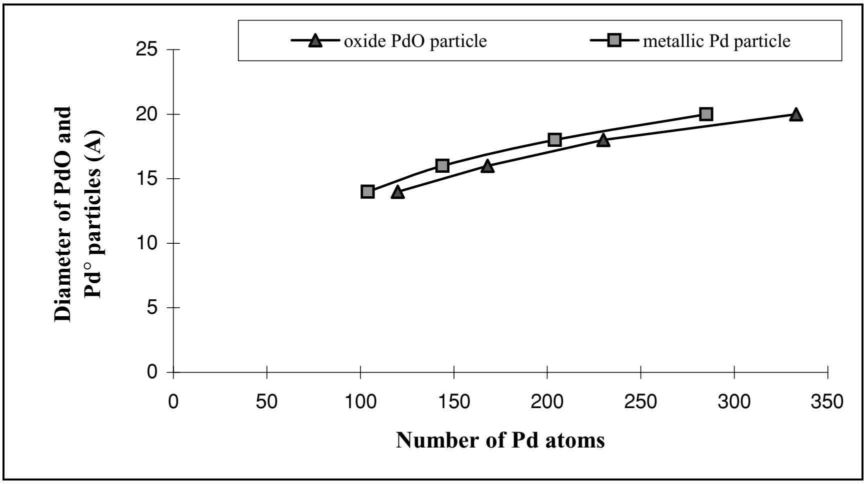

FIGURE 13.26. Number of Pd atoms in a spherical particle PdO and Pd° for different sizes.

13.3. BIMETALLIC CATALYSTS PREPARED BY COLLOIDAL SYNTHESIS

13.3.1. Palladium–Tin Catalysts

As mentioned in the introduction, the idea is to first synthesize a hydrosol (PdO, SnO_2), and then contacting it with a stannate (or palladate) complex aqueous solution. The initial oxide suspension acts as a "nano" carrier for the second element.

In the following section, we describe the case of adsorption of a Sn^{IV} complex onto a palladium oxide suspension. In an alkaline medium (a basic PdO hydrosol), chlorides in the $SnCl_4$ complex are substituted in the coordination sphere of tin(IV) by hydroxo anions, which are in excess, yielding the stannate $Sn(OH)_6{}^{2-}$ complex. The ^{119}Sn Mössbauer spectroscopy spectrum of a bimetallic sol (frozen in liquid nitrogen) is compared with a true stannic solution. At the same tin concentration, it shows the changes in the Sn environment due to adsorption onto the PdO surface (Fig. 13.27). The isomer shift δ is found to be close to zero for the stannate solution and increases when contacted with the PdO suspension, indicating a modification of the coordination sphere of tin. The increase in δ can be correlated to an increase in the core level electronic density of tin. The quadrupole splitting Δ, is related to a modification of the symmetry of the close environment of tin, due to adsorption of $Sn(OH)_6{}^{2-}$ complexes onto the PdO colloidal nanoparticles.

At pH close to 12, the surface of palladium oxide is negatively charged (point of zero charge: PIE $= 4.5$) excluding an electrostatic adsorption of the stannate anion to form an outer sphere complex. According to the multisite complexation model (MUSIC), in the investigated range of alkaline pH values, two surface hydroxyl groups are supposed to coexist, Pd_2–OH^0 (μ^2 sites) and Pd_3–$O^{-0.5}$ (μ^3 sites), yielding a negatively charged surface. Adsorption is suggested to proceed via chemisorption

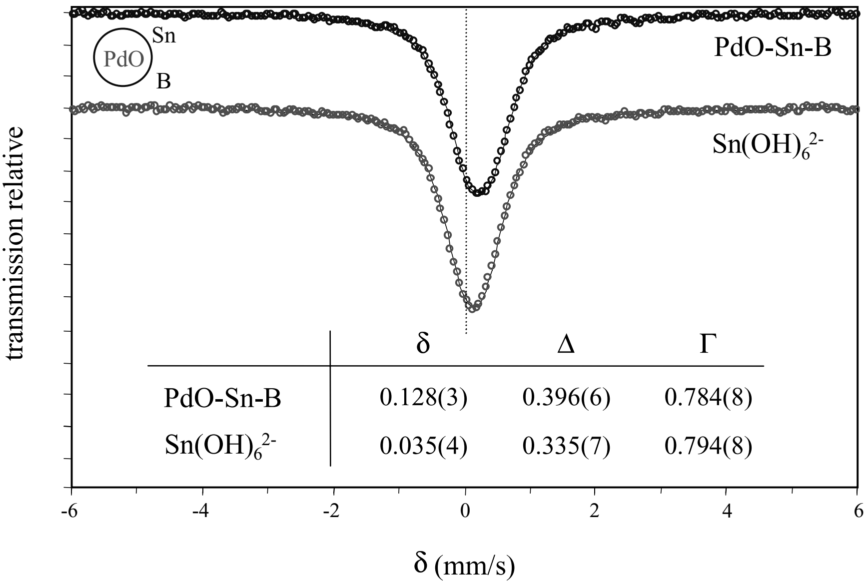

FIGURE 13.27. ^{119}Sn Mössbauer spectra at –193°C of (•) the $Sn(OH)_6^{2-}$ solution and of (○) the bimetallic *PdOSn* sol (PdO sol+$Sn(OH)_6^{2-}$) at the same tin concentration ([Sn] $= 1.3 \times 10^{-2}$ mol/L).

(hydrolytic adsorption) of stannate, leading to the formation of an inner sphere complex[41], as described in Eq. (4):

$$Pd_2{-}OH^0 + HO{-}Sn(OH)_5{}^{2-} \quad \rightarrow \quad Pd_2{-}O{-}Sn{-}(OH)_5{}^{2-} + H_2O. \qquad (4)$$

After deposition on the alumina support using a classical incipient wetness impregnation, only isolated particles are observed by TEM (Fig. 13.28). When compared to the starting PdO particles (mean particle size = 1.8 nm), the mean particle size slightly increases to 2.9 nm but the standard deviation of the distribution is kept constant.

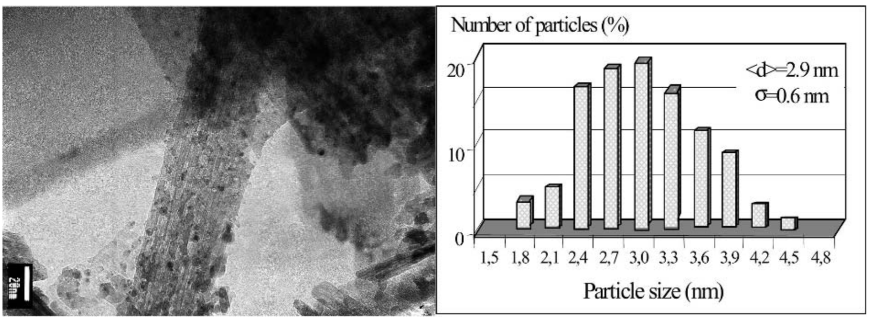

FIGURE 13.28. TEM micrograph and histogram of the *PdOSn* catalyst and particle size distribution.

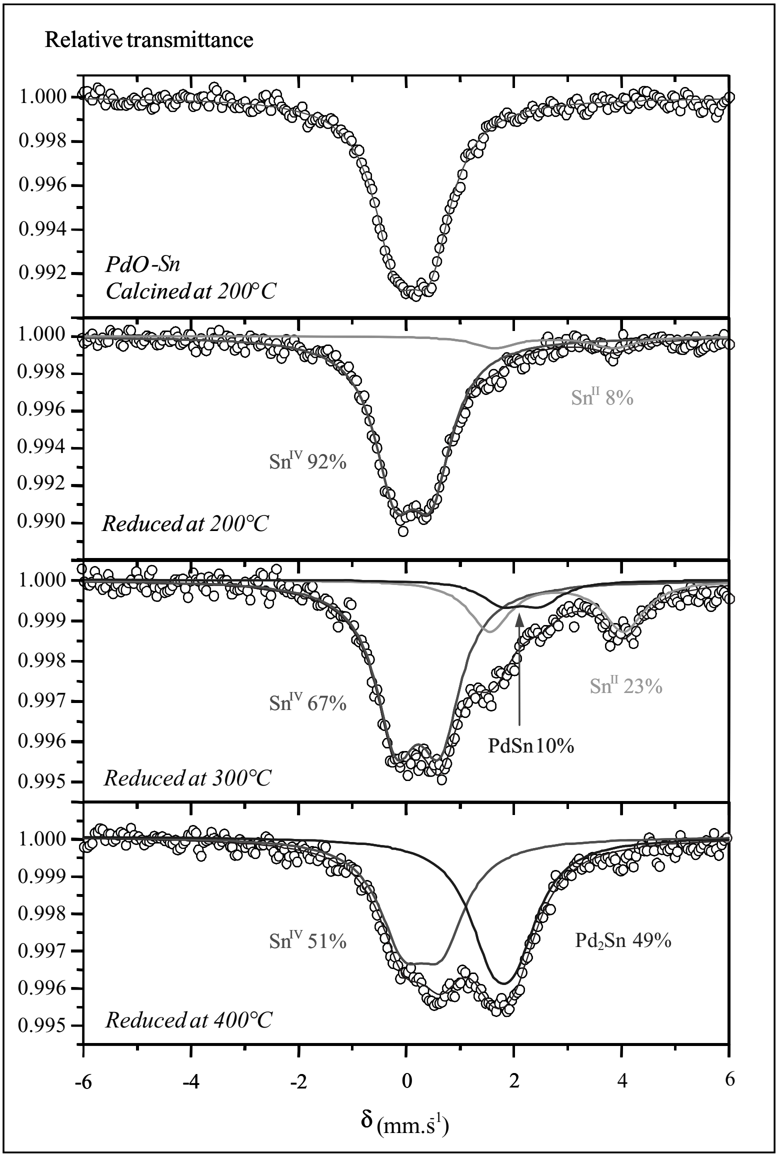

FIGURE 13.29. ^{119}Sn Mössbauer spectra of the *PdOSn* catalyst calcined at 200°C (top) and reduced at 200°C, 300°C, and 400°C (bottom).

The ^{119}Sn Mössbauer spectra of the supported catalyst (*PdOSn)* after low temperature calcination (200°C) under airflow and reduction treatments performed at different temperatures are presented in Fig. 13.29. The corresponding hyperfine parameters (δ and Δ) are reported in Table 13.2. For a reduction temperature of 200°C, the tin reduction is initiated as demonstrated by the presence of 8% of Sn^{II}. Formation of bimetallic species (presence of Pd° and Sn°) starts at around 300°C and increases with reduction

TABLE 13.2. Hyperfine parameters of refined spectra of the *PdOSn* catalyst after calcination at 200°C and reduction at various temperatures.

Sample	δ (mm/s)	Δ(mm/s)	Γ (mm/s)	RC (%)	Sn species
PdOSn Calcined at 200°C	0.02 (1)	0.62 (1)	0.98 (2)	100	Sn^{IV}
PdOSn	0.02 (1)	0.67 (1)	0.94 (2)	92	Sn^{IV}
Reduced at 200°C	2.64 (9)	2.2 (1)	1.0 (2)	8	Sn^{II}
PdOSn	0.12 (1)	0.80 (1)	0.94 (3)	67	Sn^{IV}
Reduced at 300°C	2.05 (8)	0.7 (1)	0.94 (3)	10	PdSn
	2.69 (4)	2.49 (6)	0.94 (3)	23	Sn^{II}
PdOSn	0.19 (2)	0.71 (3)	1.09 (4)	51	Sn^{IV}
Reduced at 400°C	1.70 (3)	0.44 (5)	1.09 (4)	49	Pd_2Sn

temperature: 10% of PdSn at 300°C and 49% of the expected Pd_2Sn alloy at 400°C with a molar Pd/Sn ratio close to 2. Hence, the maximum amount of Pd_2Sn observed (49%) approximately corresponds to 50% of the total amount of palladium. Stannous tin is an intermediate species between stannic tin and reduced tin and acts as a precursor of the bimetallic Pd–Sn species. As tin is supposed to migrate easily on alumina because of its ability to reoxidize via formation of tin aluminate,[42] its incorporation into palladium demonstrates that the stannate anions adsorbed on the PdO particles in the initial hydrosol is not significantly disturbed by the deposition process onto the support.

Casting microprobe analysis (Fig. 13.30) shows the very pronounced eggshell repartition of Pd and Sn across the diameter of the alumina beads. This is an important feature in the case of intragranular limited reactions such as selective hydrogenations. The thickness of the shell is very small (about 50 μm) and both elements are located in the same zone, which is a necessary condition for an interaction between the two metals.

Surface concentrations deduced from low-energy ion scattering (LEIS) spectra analysis showed that as erosion increases with time, the concentration of palladium increases whereas that of tin decreases. This result is in agreement with a pronounced surface enrichment by tin with respect to palladium according to the principle of the preparation method.

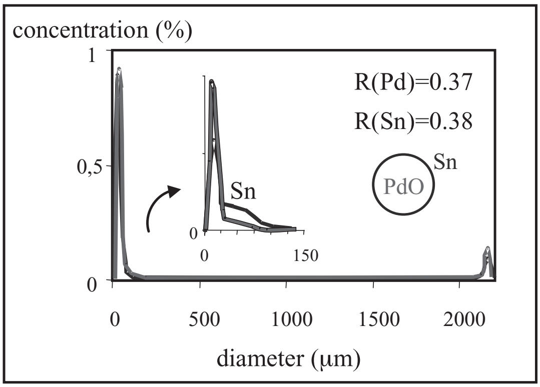

FIGURE 13.30. Repartitions of Pd and Sn obtained by casting μ probe analysis for the PdOSn catalyst (PdO—Sn).

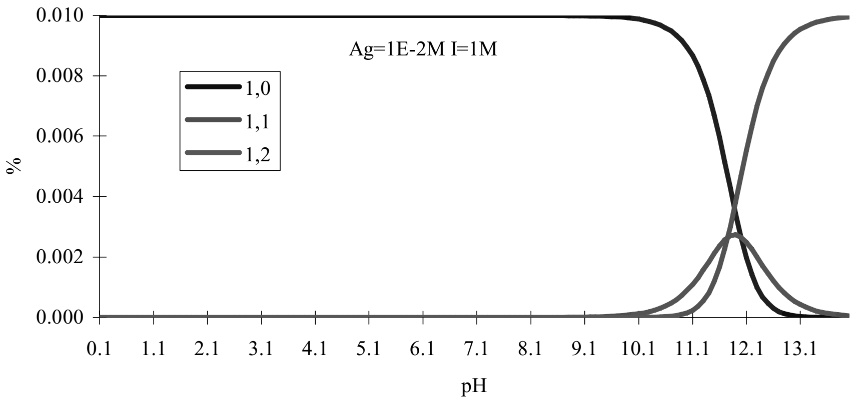

FIGURE 13.31. Predominance diagram of Ag(I): [Ag(I)] = 0.01 M I = 1 M.

13.3.2. Palladium–Silver Catalysts

Adsorption of Ag on the surface of PdO is also an interesting option offered by colloidal oxide synthesis. Silver is a well-known promoter for the improvement of catalytic properties, primarily selectivity, in various reactions such as hydrogenation of polyunsaturated compounds.[43] The more stable oxidation state of silver is +1.[44] Aquo soluble precursors are silver nitrate (halide precursors are all insoluble), and some organics such as acetate or oxalate with limited solubility may also be used.[45] Ag^+ is a d^{10} ion and can easily form linear AgL_2 type complexes according to crystal field theory. Nevertheless, even for a concentrated solution of $AgNO_3$, Ag^+ does not form aquo complexes.[46] Although a solvation sphere surrounds the cation, no metal–water chemical bonds have been observed.

The diagram presented in Fig. 13.31 is rather simple and is quite independent to the concentration of metallic precursor or ionic strength. It was obtained from the literature data[47] resolving Eq. (5.2), which was obtained from Eq. (5.1).

$$C_0 = [Ag^+] + [AgOH] + [Ag(OH)_2{}^-], \tag{5.1}$$

$$C_0 = [Ag^+] \cdot \left(1 + \frac{Q_{11}}{h} + \frac{Q_{12}}{h^2}\right), \tag{5.2}$$

where

$$Q11 = \frac{[Ag(OH)][H^+]}{[Ag^+]}, \quad \text{and} \quad Q12 = \frac{[Ag(OH)_2{}^-][H^+]^2}{[Ag^+]}.$$

If one considers now different options to generate interaction in solution between Ag^+ and the PdO surface, Fig. 13.32 shows that in the pH = 5 to 10 range electrostatic adsorption is expected to take place. In this pH range, deprotonated hydroxyl groups of the PdO surface have a negative charge and can interact with the Ag^+ cations.

Despite that thermodynamics predicts the coexistence of molecular Ag^+ and PdO oxide particles over a rather large pH domain, AgOH is readily formed at $5 < pH < 13$.

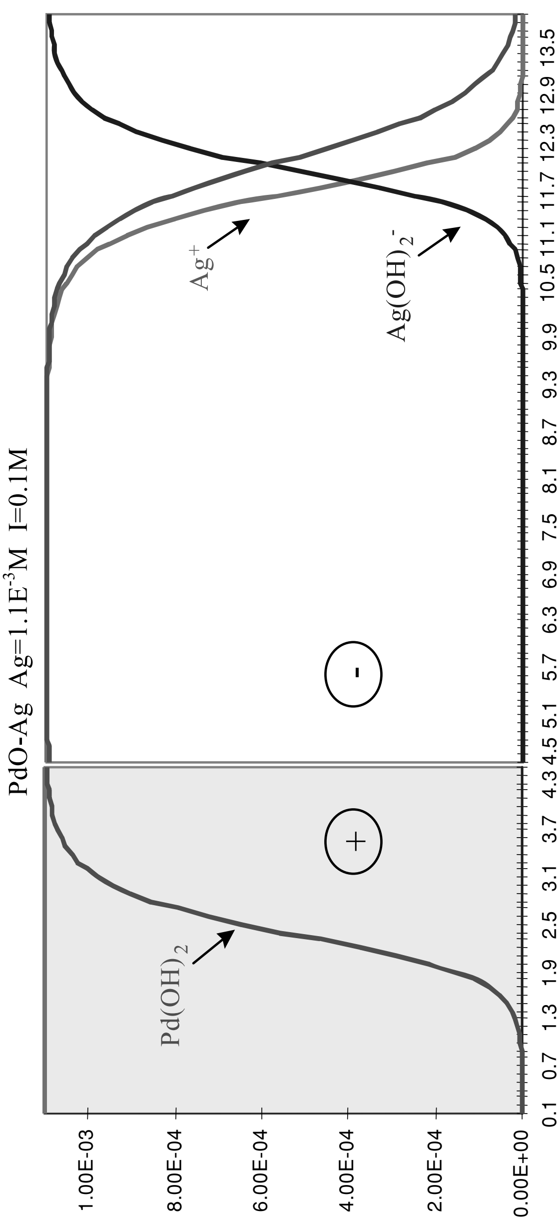

FIGURE 13.32. A predominance diagram of silver and palladium species as a function of pH.

In fact, adsorption of Ag^+ can be successfully performed by an ionic exchange mechanism for pH ≤ 5. A negatively charged PdO surface is able to adsorb Ag^+ in this acidic medium. Such a solution was impregnated onto α-Al_2O_3 and results of the catalytic tests are presented in Section 13.4.3.

13.4. APPLICATION TO CATALYSIS: SELECTIVE HYDROGENATION REACTIONS

13.4.1. Hydrogenation of Phenylacetylene on Pd Monometallic Catalysts

This section presents the result of the catalytic performances in the case of phenylacetylene hydrogenation reaction. The catalytic evaluation was performed in a classical well-stirred stainless steel reactor operating in batch mode under constant H_2 pressure (10 bar) at 17°C using n-heptane as the solvent. As mentioned in Section 13.2.2, no modification of the particle size distribution has been observed by transmission electron microscopy before or after reduction of colloidal oxide particles.

For all catalysts, the hydrogenation mechanism performed under our conditions (liquid phase and low hydrogen pressure) is consistent with an Horiuti–Polanyi mechanism.[48] We found that the phenylacetylene (PhAc) hydrogenation reaction was zero order with respect to hydrocarbon reactants up to 80% of conversion, in agreement with several other studies devoted to the hydrogenation of polyunsaturated compounds.[49]

Constant rates k (mol/s·gPd^{-1}) have been determined from the slope of the experimental curves plotting acetylenic molar concentration versus time. Turn over numbers (TONs = mol/s·atom Pd^{-1}) were calculated from the following equation:

$$\mathrm{TON} = \frac{kM}{D},$$

where M is the atomic weight of Pd, D is the dispersion defined as the fraction of exposed Pd atoms (the ratio between the number of surface atoms and the total number of atoms) obtained from CO chemisorption measurements

Catalytic results reported in Table 13.3 show a comparison between a "colloidal" catalyst and a more conventional preparation procedure using palladium acetylacetonate as a precursor.[50] These two catalysts have nearly the same dispersion, but the colloidal-based catalyst is roughly six times more active for PhAc hydrogenation.

Particle size distribution of the catalysts prepared from acetylacetonate (Fig. 13.33) reveals a much larger distribution than that of the catalyst prepared from the colloidal route (Fig. 13.23b). This difference may explain the relatively poor specific activity

TABLE 13.3. Characteristics and catalytic activity of samples prepared from the colloidal method and conventional preparation method.

	Particle Size (Å) (TEM)	Particle Size Distribution (TEM)	Dispersion % by CO Chemisorption	k PhAc mol/s^{-1}·gPd^{-1}	TON PhAc mol/s·atom Pd^{-1}
"Colloidal" catalyst	19	Narrow $\sigma = 4$	63	0.052	8.8
Preparation using $Pd(Acac)_2$	23	Broad $\sigma = 8.1$	66	0.008	1.3

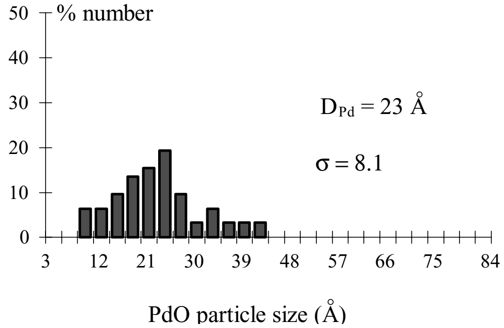

FIGURE 13.33. Particle size distribution obtained by TEM analysis of the $Pd(Ac)_2$ catalyst.

of the catalyst containing small particles (<10 Å), which have a low activity for such a highly structure sensitive reaction, and large particles (>30 Å), which have a low fraction of accessible atoms. Thus, the highest hydrogenation activity is obtained for particle sizes between 10 and 30 Å.

Regarding the degree of aggregation, a comparison of the catalytic activity of the two "colloidal" catalysts is given in Table 13.4. It appears that the aggregation of particles lowers the specific activity of the catalyst but the turn over number is significantly higher for the catalyst having aggregated particles (Fig. 13.34). The same observation has been made for butadiene hydrogenation.

An infrared study of adsorbed CO showed that particle aggregation occurred mainly at unsaturated atoms sites such as corners and edges. These low coordination atoms are then blocked to the reactants, which can only be activated by atoms located on planes. Moreover, the binding energy of the $3d_{5/2}$ core level, determined by X-ray photoelectron spectroscopy (XPS) of aggregated particles ($El_{3d5/2} = 334.4$ eV), is smaller than that of isolated particles of 20 Å in size ($El_{3d5/2} = 334.8$ eV) (Fig. 13.34). In summary, aggregation phenomenon promotes geometric and electronic effects in such a way that an increase of the TON is observed due to a favorable organization of the particles on the surface of the support, leading to the blocking of the unsaturated atoms having a lower intrinsic hydrogenation activity.[51]

13.4.2. Hydrogenation of Butadiene on Bimetallic Palladium–Tin Catalysts

A colloidal suspension prepared according to the method described in Section 13.2.3 was contacted with a porous alumina carrier to obtain a bimetallic palladium–tin catalyst. Evaluation of the catalytic properties of this system is detailed

TABLE 13.4. Characteristics and catalytic activity of samples prepared from colloidal suspensions.

Particle Size (Å) (by TEM)	TEM Observation	Dispersion % by CO Measurements	k PhAc mol/s·gPd^{-1}	TON PhAc mol/s ·atom Pd^{-1}
20	Aggregated particles	12	0.033	29.3
19	Isolated particles	63	0.052	8.8

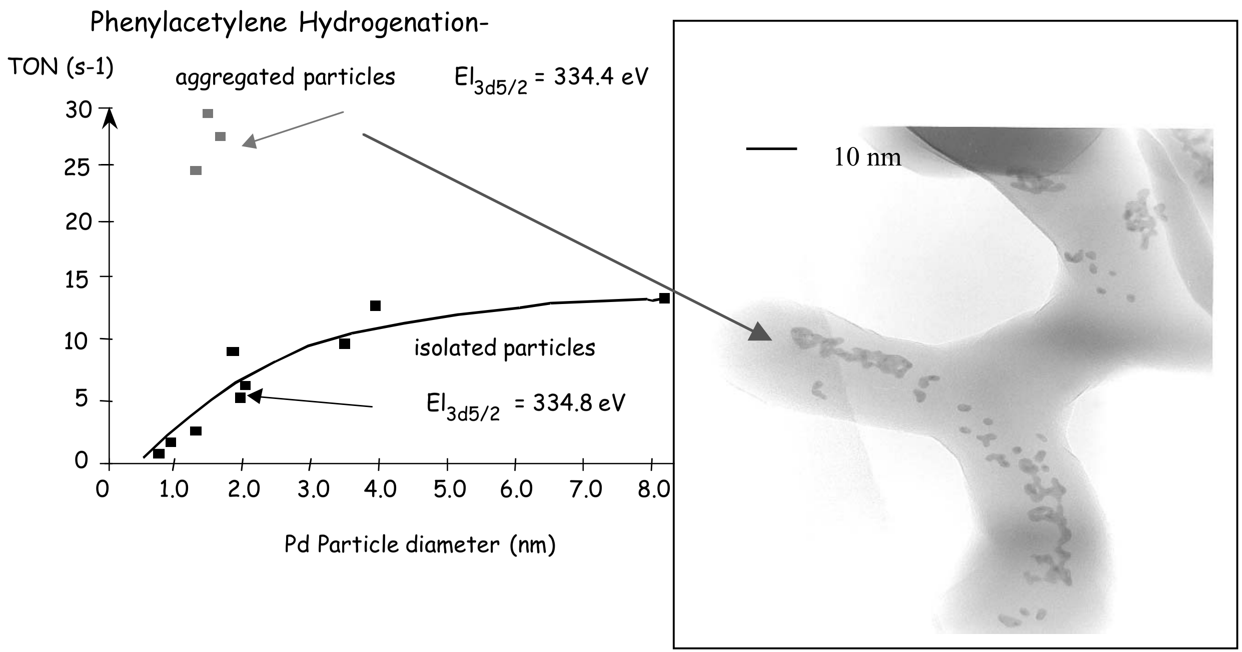

FIGURE 13.34. Comparison of phenylacetylene hydrogenation TON for aggregated and isolated Pd on α-Al_2O_3 particles.

TABLE 13.5. Intrinsic kinetic constant k_i (mol/s·mol$_{\text{surface Pd}}$$^{-1}$) and kinetic selectivity r for different catalysts after reduction at 200°C.

$T_{red} = 200°C$	PdO	PdSn	PdOSn
k_1 (BD→B1)	5.8	8.2	11.6
k_2 (BD→B2)	3.6	2.4	6.6
k_3 (B1→BA)	2.6	7.3	2.3
k_4 (B1→B2)	4.7	8.9	2.5
$K_{BD}/K_{Butenes}$	22.0	11.2	80.9
r	17.3	5.7	194.4

hereafter in the case of buta-1,3-diene hydrogenation in liquid phase, and compared to a bimetallic catalyst obtained via a standard procedure of coimpregnation of palladium and tin precursors.

Buta-1,3-diene (BD) hydrogenation is a widely used model reaction to investigate surface modification by promoters or alloy formation.[52] The reaction is usually described as a consecutive mechanism[53,54] without direct hydrogenation of buta-1, 3-diene to butane (BA).[55]

From the kinetic and adsorption constants, the kinetic selectivity r is defined as

$$r = \frac{k_1.K_{BD}}{(k_3 + k_4).K_{B1}} \quad \text{for the reaction mechanism} \quad BD \xrightarrow{k_1} B1 \begin{cases} \xrightarrow{k_3} BA \\ \xrightarrow{k_4} B2 \end{cases}$$

More details concerning calculation of the kinetic parameters are given in Ref. 56.

In the results presented in Table 13.5, the addition of tin affects the kinetic selectivity r differently, depending on the catalyst preparation method. When compared to the monometallic PdO catalyst, r slightly decreases for the coimpregnated PdSn catalyst, but it sharply increases for the PdOSn catalyst prepared via the colloidal oxide synthesis. As the intrinsic kinetic constant rates k_i do not show significant discrepancies between the different catalysts, the main contribution of the variation of the kinetic selectivity is ascribed to the adsorption constant ratio $K_{BD}/K_{Butenes}$. In the case of the PdOSn catalyst, formation of but-1-ene is favored compared to its consumption because the $K_{BD}/K_{Butenes}$ ratio increases, indicating that olefin adsorption is much more destabilized than diene adsorption. Thus, the olefin easily desorbs before being hydrogenated into butane.

In short, it has been observed that aggregation of particles plays an important role for the catalytic properties. For the same reduction temperature ($T_{red} = 200°C$) aggregated particles are much more selective ($r = 194$ versus 27) for the same amount of Pd_2Sn phase (around 40%). In this case, the change of selectivity cannot be related to the amount of Pd_xSn_y alloy. This shows that the degree of aggregation of the supported particles plays a major role in controlling the kinetic selectivity of the catalyst through the adsorption constant ratio $K_{BD}/K_{Butenes}$. On the other hand, the aggregation state does not modify the intrinsic constant rates k_i.

In the case of isolated particles, the kinetic selectivity increases with the reduction temperature (Fig. 13.35). In this case, the $K_{BD}/K_{Butenes}$ ratio remains almost constant, but the intrinsic kinetic constants relative to the hydrogenation and double bond

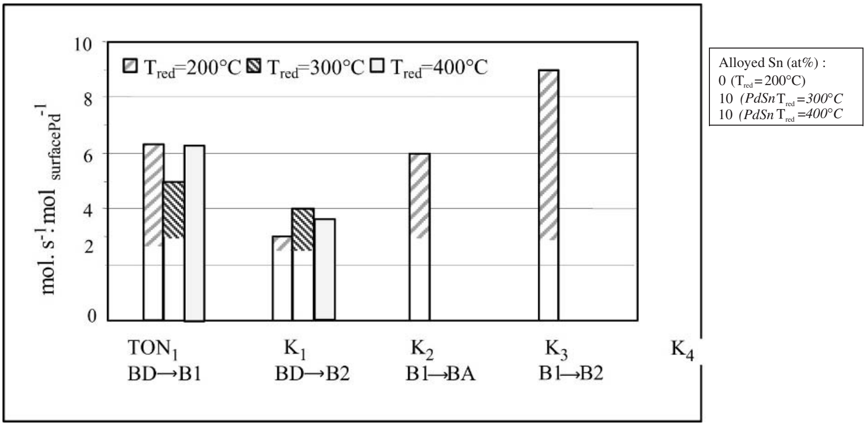

FIGURE 13.35. Effect of reduction temperature on kinetic constants and % of alloyed phases determined by ^{119}Sn Mössbauer spectroscopy.

isomerization of but-1-ene (k_3 and k_4 respectively) decreases sharply. When the reduction temperature increases, the aggregation state does not vary; the supported metallic particles remain isolated without sintering. Thus, the modification of the chemical steps relative to but-1-ene can be associated with the increasing proportion of Sn$^\circ$ incorporated in the alloyed phase changing the electronic properties of active sites as shown by different characterization techniques (XPS and IR of adsorbed CO).[56]

13.4.3. Hydrogenation of Acetylene on Bimetallic Palladium–Silver Catalysts

A supported PdAg/α-Al_2O_3 bimetallic catalyst prepared according to the colloidal method described in Section 13.3.2 was characterized and tested for acetylene/ethylene hydrogenation in typical tail end gas phase conditions ($P_{tot} = 25$ bar, $H_2/C_2H_2 = 1.5$ mol/mol, 2% C_2H_2 in C_2H_4, WHSV $= 3000\ h^{-1}$). Figure 13.36 shows the increase in the time corresponding to the breakthrough of acetylene compared to a Pd monometallic catalyst and a PdAg catalyst with the same composition prepared with a conventional incipient wetness coimpregnation method.

High bimetallic character at a nanometer scale is probably the reason of this spectacular change in performance. As proposed in reference[57], the formation of heavy oligomers (green oil), which is the main deactivation factor and responsible of the acetylene breakthrough, is strongly inhibited on the surface of the bimetallic catalyst due to the isolation of adsorption sites. The probability of coupling between carbene or carbyne fragments covering the metallic surface is much lower on a bimetallic surface, increasing the cycle length and ethylene yields.

13.5. CONCLUSION

In this chapter, we discussed some general results obtained using a new route of preparation method of metallic supported catalysts by using colloidal oxide chemistry

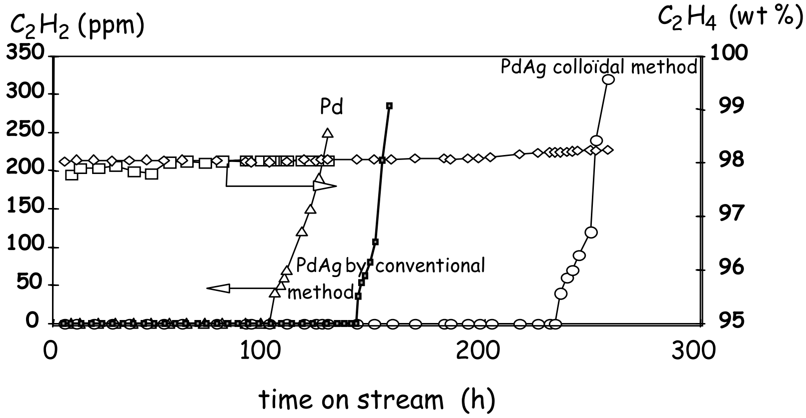

FIGURE 13.36. Yields in C_2H_2 and C_2H_4 versus time on stream for a Pd monometallic and PdAg bimetallic catalysts.

in aqueous phase. It has been shown that this method can be successfully applied to control the physical and chemical characteristics of supported particles at a nanometer scale, including particle size distribution, repartition on the support, and the interaction between metals in the case of multimetallic formulations. The fundamental bases of this chemistry follow the general principles already described for other oxides, but a real predictive approach of the phenomenon needs to take into account the kinetic factors governing the different reactions involved (nuclei formation and growth, dissolution, and aggregation), and which are specific of each system (nature of the metal, precursors, pH, metal concentration).

The catalytic performances of the supported catalysts clearly demonstrated the improvement in terms of activity or selectivity by such optimized catalytic systems. This improvement is related to a nanometer control of the critical characteristics of the active sites. Enhancement of the catalytic performances and the understanding of structure–reactivity relationships can only be achieved by advancing the understanding of different preparation methods, eventually leading to better control over the characteristics of the active sites at a nanometer scale. Moreover, new properties of these solids may be found, which could have a great impact on catalytic reactions.

REFERENCES

1. M. Che, O Clause, and Ch. Marcilly, Deposition of active component In *Preparation of Solid Catalysts*, edited by G. Ertl, H. Knözinger, and J. Weitkamp (Wiley-VCH, Weinheim 1999) pp. 315–340.
2. C. Louis, and M. Che, Anchoring and grafting of coordination metal complexes onto oxide surfaces In *Preparation of Solid Catalysts* edited by G. Ertl, H. Knözinger, and J. Weitkamp (Wiley-VCH, Weinheim 1999) pp. 341–371.
3. J. A. Rob van Veen, G. Jonkers, and W. H. Hesselink, Interaction of transition-metal acetylacetonates with γ-Al_2O_3 surfaces, *J. Chem. Soc. Faraday Trans.* 1 **85**(2), 389–413 (1989).
4. YU. I. Yermakov, Supported catalysts obtained by interaction of organometallic compounds of transition elements with oxide supports, *Catal. Rev. Sci. Eng.* **13**(1), 77–120 (1976).

5. M. Schreier, and J. R. Regalbuto, A fundamental study of Pt tetra ammine impregnation of silica 1: The electrostatic nature of platinum adsorption, *J. Catal.* **225,** 190–202 (2004).
6. M. Boudart, Catalysis by supported metals, In *Advances in Catalysis*, vol. 20, (Academic Press, San Diego 1969) pp. 153–166.
7. P. W. Jacobs, and G. A. Somorjai, Conversion of heterogeneous catalysis from art to science: The surface science of heterogeneous catalysis, *J. Mol. Catal. A Chem.* **131,** 5–18 (1998).
8. M. Che, and C. O. Bennett, The influence of particle size on the catalytic properties of supported metals, In *Advances in Catalysis*, vol. 36, (Academic Press , San Diego 1989) pp. 55–172.
9. V. Ponec, anjd G. C. Bond, Catalysis by metals and alloys, *Stud. Surf. Sci. Catal.* **95,** 317 (1995).
10. E. Lamy-Pitara, and J. Barbier, Platinum modified by electrochemical deposition of adatoms, *Appl. Catal.* A **149,** 49–87 (1997).
11. C. Micheaud, P. Marécot, M. Guérin, and J. Barbier, Preparation of alumina supported palladium-platinum catalysts by surface redox reactions: Activity for complete hydrocarbon oxidation, *Appl. Catal.* A **171,** 229–239 (1998).
12. J. Barbier, Redox method of bimetallic catalysts, In *Handbook of Heterogeneous Catalysis* edited by G. Ertl, H. Knözinger, and J. Weitkamp (Wiley-VCH, Weinheim 1997) pp. 257–264.
13. J. Margitfalvi, S. Szabó, and F. Nagy, Supported bimetallic catalysts prepared by controlled surface reactions, *Stud. Surf. Sci. Catal.* **27,** 373–409 (1983).
14. Y. A. Ryndin, and Y. I. Yermakov, Reactions of organometallic compounds with surfaces of supported and unsupported metals, In *Surface Organometallic Chemistry: Molecular Approaches to Catalysis* edited by J. -M. Basset, B. C. Gates, J.-P. Candy, A. Choplin, M. Lecomte, F. Quignard, and C. Santini (Kluwer, Dordrecht 1998) pp. 127–141.
15. J. P. Candy, B. Didillon, E. L. Smith, T. M. Shay, and J. M. Basset, Surface organometallic chemistry on metals: A novel and effective route to custom-designed bimetallic catalysts, *J. Mol. Catal.* **86,** 179–204 (1994).
16. A. Goguet, M. Aouine, F. J. Cadete Santos Aires, A. De Malmann, D. Schweich, and J. P. Candy, Preparation of a Pt/SiO_2 catalyst, *J. Catal.* **209,** 135–144 (2002).
17. N. Yao, C. Pinckney, S. Lim, C. Pak, and G. L Haller, Synthesis and characterization of Pt/MCM-41 catalysts *Microporous Mater.* **44–45,** 377–384 (2001).
18. J. Livage, and C. Sanchez, Sol–gel chemistry *J. Non Crystalline Solids* **145**(1–3), 11 (1992).
19. C. J. Brinker, and G. W. Scherer, Sol–gel science: The physics and chemistry of sol–gel processing, In *Sol–Gel Science*, (Academic Press, San Diego 1990) pp. 907, 108.
20. J. P Jolivet, In *De la Solution à l'oxyde* edited by CNRS, (1994).
21. L. N. Lewis, and N. Lewis, Platinum catalyzed hydrosilylation—Colloid formation as the essential step, *J. Am. Chem. Soc.* **108,** 7228–7231 (1986).
22. H. Bonnemann, W. Brijoux, R. Brinkmann, E. Dinjus, T. Jouben, R. Fretzen, and B. Korall, Highly dispersed metal clusters and colloïds for the preparation of active liquid-phase hydrogenation catalysts, *J. Mol. Catal*. **74,** 323–333 (1992).
23. J. Belloni, Metal nanocolloids, *Colloid Interface Sci.* **1**(2), 184–196 (1996).
24. A. Rakai, D. Tessier, and F. Bozon-Verduraz, Palladium-alumina catalysts: A diffuse reflectance study, *New J. Chem.* **16,** 869–875 (1992).
25. L. I. Elding, and L. F. Olsson, Electronic absorption spectra of square-planar chloro-aqua and bromo-aqua complexes of palladium (II) and platinum (II), *J. Phys. Chem.* **82**(1), 69–74 (1978)
26. P. B. Critchlow, and S. D. Robinson, A review of platinum metal nitrato complexes, *Coord. Chem. Rev.* **25**(1), 69–102 (1978)
27. J. P. Jolivet, In *De la solution à l'oxyde* edited by CNRS, (1994) pp. 219—254.
28. T. Hiemstra, W. H. van Riemsdijk, and G. H. Bolt, Multisite proton adsorption modeling at the solid/solution interface of (hydr)oxides: A new approach: I. Model description and evaluation of intrinsic reaction constants, *J. Colloid Interface Sci.* **133**(1), 99–104 (1989).
29. J. P. Jolivet, In *De la solution à l'oxyde* edited by CNRS, (1994) pp. 52—64.
30. J. P. Jolivet, In *Metal Oxide Chemistry and Synthesis, from Solution to Solid State* edited by Wiley & Sons, (Wiley & Sons, New York 2000), p. 223.
31. R. Sprycha, Surface charge and adsorption of background electrolyte ions at anatase/electrolyte interface, *J. Colloid Interface Sci.* **102**(1), 173 (1984).

32. B. N. Ivanov-Emin, B. E. Zaitsev, L. P. Petrishcheva, T. M. Ivanova, and R. V. Lin'ko, Study of alkaline solutions of palladium (II) oxide hydrate, *Russ. J. Inorg. Chem.* **30,** 1786 (1985).
33. S. Desset, O. Spalla, and B. Cabane, Redispersion of alumina particles in water, *Langmuir* **16,** 10495–10508 (2000).
34. D. Fauchadour, *PhD Thesis* Orléans University (2000).
35. B. I. Nabivanets, L. V. Kalabina, State of palladium (II) and platinum (IV) in inorganic acid solutions, *Russ. J. Inorg. Chem.* **15,** 818 (1970).
36. C. F. Baes, R.E. Mesmer, In *The Hydrolysis of Cations*, edited by John Wiley & Sons (Wiley & Sons, New York 1976).
37. E. Matijevic, Production of monodispersed colloidal particles, *Ann. Rev. Mater. Sci.* **15,** 483–516 (1985).
38. E. Matijevic, Monodispersed colloids: Art and science, *Langmuir* **2**(1), 12–20 (1986).
39. E. Matijevic, Preparation and properties of monodispersed colloidal metal hydrous oxides, *Pure Appl. Chem.* **50**(9–10), 1193–1210 (1978).
40. E. Matijevic, Preparation and properties of uniform size colloids, *Chem. Mater.* **5**(4), 412–426 (1993).
41. J.P. Jolivet, In *Metal Oxide Chemistry and Synthesis, from Solution to Solid State*, edited by John Wiley & Sons, (Wiley & Sons, New York 2000) p. 286.
42. T. Cholley, *PhD Thesis* University Paris VI (1997).
43. V. Ponec, and G. C. Bond, Catalysis by metals and alloys, *Stud. Surf. Sci. Catal.* **95,** 488 (1995).
44. C. F. Baes, and R. E. Mesmer, In *The Hydrolysis of Cations*, edited by John Wiley & Sons, (John Wiley & Sons, New York 1976) p. 274.
45. Gmelin's Handbook of Inorganic Chemistry, Ag [B5], p. 130.
46. Gmelin's Handbook of Inorganic Chemistry, Ag [A3], p. 70.
47. C. F. Baes, R.E. Mesmer, In *The Hydrolysis of Cations*, edited by John Wiley & Sons, (John Wiley & Sons, New York 1976) p. 276.
48. J. Horiuti, and T. Nakamura, Stoichiometric number and the theory of steady reaction, *Z. Phys. Chem.* Neue Folge **11,** 358–365 (1957).
49. G. C. Bond, In *Catalysis by Metals Chapter 12–14,* (Academic Press, London 1962) pp. 281–352.
50. J. P. Boitiaux, J. Cosyns, and S. Vasudevan, Hydrogenation of highly unsaturated hydrocarbons over highly dispersed palladium catalyst: Part I. Behaviour of small metal particles, *Appl. Catal.* **6,** 41–51 (1983).
51. Z. Karpinski, Catalysis by supported, unsupported and electron-deficient palladium, *Adv. Catal.* **37,** 45–100 (1981).
52. V. Ponec, and G. C. Bond, Catalysis by metals and alloys, *Stud. Surf. Sci. Catal.* **95,** 500 (1995).
53. J. P. Boitiaux, J. Cosyns, M. Derrien, and G. Léger, Proper design of butadiene selective hydrogenation process for maximum 1-butene yield by using comprehensive kinetic model, *AIChE National Meeting* (*Houston, March 24, 1984*).
54. J. Goetz, D. Y. Murzin, M. Ulischenko, and R. Touroude, Kinetics of buta-1,3-diene hydrogenation over palladium catalysts, *Chem. Eng. Sci.* **51**(11), 2879–2884 (1996).
55. J. P. Boitiaux, J. Cosyns, and E. Robert, Hydrogenation of unsaturated hydrocarbons in liquid phase on palladium, platinum and rhodium catalysts, *Appl. Catal.* **35,** 193 (1987).
56. S. Verdier, B. Didillon, S. Morin, and D. Uzio, $PdSn/Al_2O_3$ catalysts from colloidal oxide synthesis: II. Surface characterization and catalytic properties for buta-1,3-diene selective hydrogenation, *J. Catal.* **218,** 288–295 (2003).
57. B. Didillon, P. Sarrazin, J. P. Boitiaux, P. Vance, and Ch. Cameron, Advanced catalyst design for high ethylene production and maximized cycle lengths, *AIChE Spring Meeting* (*Houston, TX, March 19—23, 1995*), Symposium Hydroprocessing IV.